



# Mix-and-Match System for the Enzymatic Synthesis of Enantiopure Glycerol-3-Phosphate-Containing Capsule Polymer Backbones from *Actinobacillus pleuropneumoniae*, *Neisseria meningitidis*, and *Bibersteinia trehalosi*

Christa Litschko,<sup>a</sup> Insa Budde,<sup>a</sup> Monika Berger,<sup>a</sup> Andrea Bethe,<sup>a</sup> Julia Schulze,<sup>a</sup> E. Alberto Alcalá Orozco,<sup>b</sup> Reza Mahour,<sup>b\*</sup> Peter Goettig,<sup>c</sup> Jana Indra Fühling,<sup>a,d</sup> Thomas Rexer,<sup>b</sup> Rita Gerardy-Schahn,<sup>a</sup> Mario Schubert,<sup>c</sup> Timm Fiebig<sup>a</sup>

<sup>a</sup>Institute of Clinical Biochemistry, Hannover Medical School, Hannover, Germany

<sup>b</sup>Max Planck Institute for Dynamics of Complex Technical Systems, Bioprocess Engineering, Magdeburg, Germany

<sup>c</sup>Department of Biosciences, University of Salzburg, Salzburg, Austria

<sup>d</sup>Fraunhofer International Consortium for Anti-Infective Research (ICAIR), Hannover, Germany

**ABSTRACT** Capsule polymers are crucial virulence factors of pathogenic bacteria and are used as antigens in glycoconjugate vaccine formulations. Some Gram-negative pathogens express poly(glycosylglycerol phosphate) capsule polymers that resemble Gram-positive wall teichoic acids and are synthesized by TagF-like capsule polymerases. So far, the biotechnological use of these enzymes for vaccine developmental studies was restricted by the unavailability of enantiopure CDP-glycerol, one of the donor substrates required for polymer assembly. Here, we use CTP:glycerol-phosphate cytidylyltransferases (GCTs) and TagF-like polymerases to synthesize the poly(glycosylglycerol phosphate) capsule polymer backbones of the porcine pathogen *Actinobacillus pleuropneumoniae*, serotypes 3 and 7 (*App3* and *App7*). GCT activity was confirmed by high-performance liquid chromatography, and polymers were analyzed using comprehensive nuclear magnetic resonance studies. Solid-phase synthesis protocols were established to allow potential scale-up of polymer production. In addition, one-pot reactions exploiting glycerol-kinase allowed us to start the reaction from inexpensive, widely available substrates. Finally, this study highlights that multidomain TagF-like polymerases can be transformed by mutagenesis of active site residues into single-action transferases, which in turn can act in *trans* to build-up structurally new polymers. Overall, our protocols provide enantiopure, nature-identical capsule polymer backbones from *App2*, *App3*, *App7*, *App9*, and *App11*, *Neisseria meningitidis* serogroup H, and *Bibersteinia trehalosi* serotypes T3 and T15.

**IMPORTANCE** Economic synthesis platforms for the production of animal vaccines could help reduce the overuse and misuse of antibiotics in animal husbandry, which contributes greatly to the increase of antibiotic resistance. Here, we describe a highly versatile, easy-to-use mix-and-match toolbox for the generation of glycerol-phosphate-containing capsule polymers that can serve as antigens in glycoconjugate vaccines against *Actinobacillus pleuropneumoniae* and *Bibersteinia trehalosi*, two pathogens causing considerable economic loss in the swine, sheep, and cattle industries. We have established scalable protocols for the exploitation of a versatile enzymatic cascade with modular architecture, starting with the preparative-scale production of enantiopure CDP-glycerol, a precursor for a multitude of bacterial surface structures. Thereby, our approach not only allows the synthesis of capsule polymers but might also be exploitable for the (chemo)enzymatic synthesis of other glycerol-phosphate-containing structures such as Gram-positive wall teichoic acids or lipoteichoic acids.

**Citation** Litschko C, Budde I, Berger M, Bethe A, Schulze J, Alcalá Orozco EA, Mahour R, Goettig P, Fühling JI, Rexer T, Gerardy-Schahn R, Schubert M, Fiebig T. 2021. Mix-and-match system for the enzymatic synthesis of enantiopure glycerol-3-phosphate-containing capsule polymer backbones from *Actinobacillus pleuropneumoniae*, *Neisseria meningitidis*, and *Bibersteinia trehalosi*. mBio 12: e00897-21. <https://doi.org/10.1128/mBio.00897-21>.

**Editor** Rino Rappuoli, GSK Vaccines

**Copyright** © 2021 Litschko et al. This is an open-access article distributed under the terms of the [Creative Commons Attribution 4.0 International license](https://creativecommons.org/licenses/by/4.0/).

Address correspondence to Timm Fiebig, Fiebig.Timm@mh-hannover.de.

\* Present address: Reza Mahour, c-Lecta GmbH, Leipzig, Germany.

**Received** 1 April 2021

**Accepted** 12 April 2021

**Published** 26 May 2021

**KEYWORDS** enzymatic synthesis, capsule, glycoconjugate vaccine, antibiotic resistance, glycerol, polysaccharides, teichoic acid, animal health, TagF-like polymerases, veterinary vaccine development, glycosyltransferase, recombinant protein expression, NMR

Multidrug-resistant bacteria are a threat to public health and the implementation of novel therapeutic or prophylactic approaches is challenging (1). One reason for increasing resistance is the use of broad-band antibiotics in animal husbandry (2). *Actinobacillus pleuropneumoniae*, a pig-specific, Gram-negative, encapsulated pathogen, and causative agent of highly contagious porcine pleuropneumonia, presents an economic burden for the swine industry worldwide and is typically treated with antibiotics (3). Although vaccines based on *A. pleuropneumoniae* toxins, attenuated strains, and subunit vaccines exist, they fail to protect against transmission (3, 4). According to a recent study (5), in herds with a high prevalence of clinical disease, the administration of a high-efficacy vaccine would be economically superior to the application of medicine. Thus, the implementation of new vaccination strategies against *A. pleuropneumoniae* could prevent the use of antibiotics and be of major advantage for global health.

Most effective antibacterial vaccine formulations contain glycoconjugates made of capsule polymers coupled to carrier proteins (6). For the conventional production of glycoconjugate vaccines, these polymers are obtained through mass cultivation of the pathogen, which requires highest biosafety standards (7), causes considerable costs, and thus prevents broad application in animal husbandry. *In vivo*, capsule polymers are synthesized by capsule polymerases before they are exported outside the cell, where they form a thick layer that protects the pathogen from the immune system of its host (8). In recent years, capsule polymerases have become attractive synthesis tools for both *in vivo* and *in vitro* synthesis systems, because their use is pathogen-free, stereoselective and regioselective, highly efficient, and even allows the buildup of large and complex structures unobtainable through chemical synthesis (9, 10). Recently, we identified a new family of capsule polymerases, the TagF-like capsule polymerase family, which is abundant in Gram-negative human and animal pathogens expressing a group 2 capsule such as *Neisseria meningitidis*, *A. pleuropneumoniae*, *Haemophilus influenzae*, *Bibersteinia trehalosi*, and *Escherichia coli* (11). Members of this family represent multidomain enzymes that generate complex phosphate-containing capsules. One subset synthesizes poly(oligosaccharide phosphate), a second subset assembles poly(glycosylpolyol phosphate), which is similar to wall teichoic acid type II (11). TagF-like capsule polymerases have a modular architecture, whose common denominator is the TagF-like fold. It transfers either glycerol- or hexose/N-acetylhexosamine-phosphate and can be paired with an N-terminal GT-A folded domain adding a hexose/N-acetylhexosamine in beta-linkage or with a C-terminal GT-B folded domain adding a hexose/N-acetylhexosamine in alpha-linkage. The latter subset includes the enzymes Cps3D and Cps7D from *A. pleuropneumoniae* serotypes 3 and 7 (*App3* and *App7*), respectively, which generate the poly(glycosylglycerol phosphate) structures  $[\rightarrow 4)\text{-}\alpha\text{-Gal-(1}\rightarrow 2)\text{-Gro-(3-PO}_4^-)]$  and  $[\rightarrow 3)\text{-}\alpha\text{-Gal-(1}\rightarrow 1)\text{-Gro-(3-PO}_4^-)]$  starting from UDP-galactose (UDP-Gal) and CDP-glycerol (CDP-Gro) (Fig. 1). Both enzymes were shown to incorporate *sn*-glycerol-1-phosphate (Gro1P) and *sn*-glycerol-3-phosphate (Gro3P) (enantiomers due to chirality at C2) from a racemic mixture of CDP-Gro into their polymer product (11), even though *in vivo*, the *App7* polymer backbone was found to exclusively contain Gro3P (12). The stereochemistry of glycerol in the *App3* polymer has not yet been analyzed (13).

In bacteria, CDP-Gro is usually synthesized by CTP:*sn*-glycerol-3-phosphate cytidyltransferases (GCTs) from the substrates CTP and Gro3P (Fig. 1b) (14). The genes *cps3B* and *cps7B*, localized in the capsule gene cluster of *A. pleuropneumoniae* serotypes 3 and 7 (Fig. 1c), respectively, were predicted to encode these enzymes (15). Enantiopure CDP-Gro is commercially not available and to the best of our knowledge,

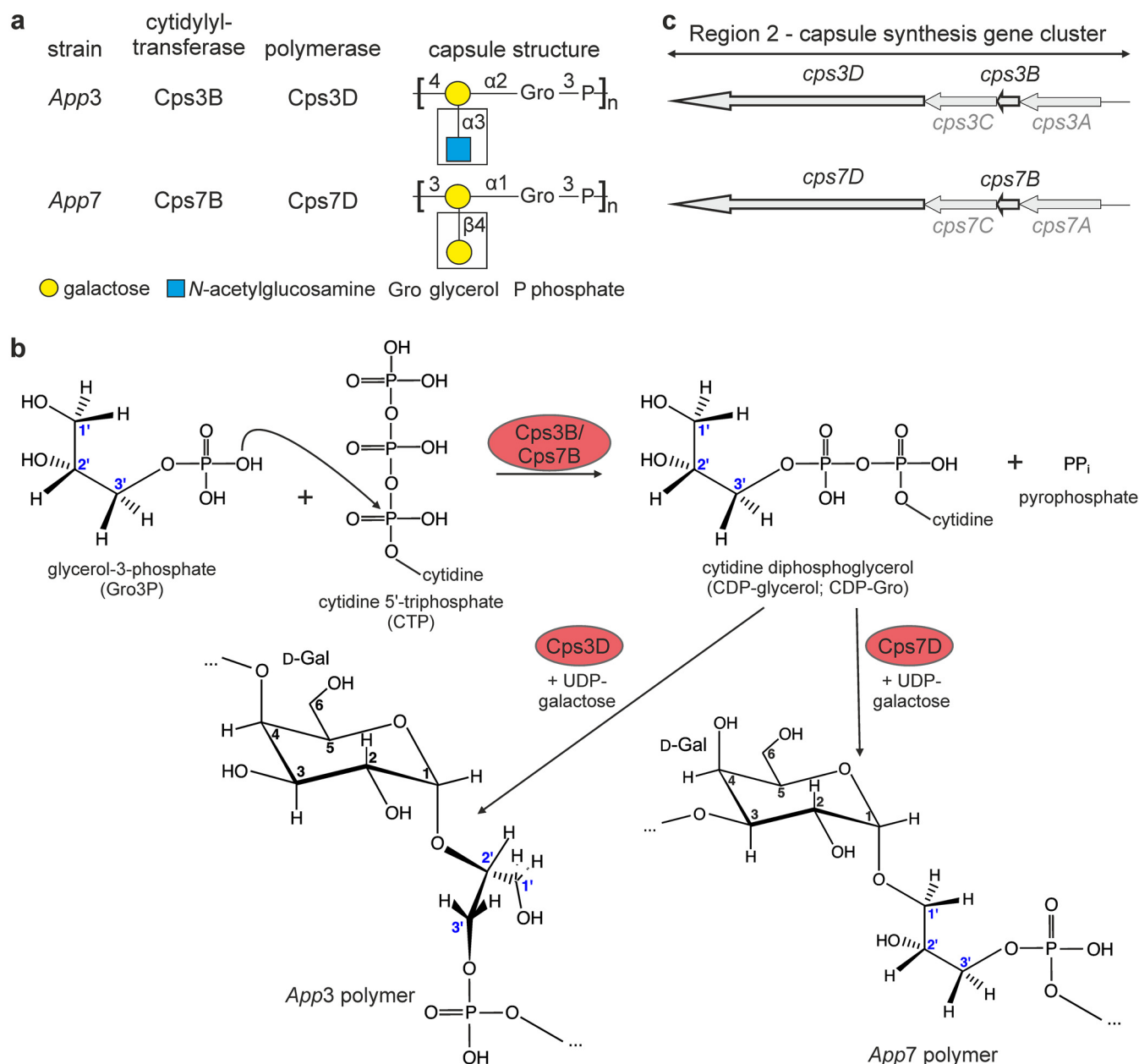


**FIG 1** Capsule synthesis in *App3* and *App7*. (a) Cytidylyltransferases (GCTs), polymerases, and capsule polymer structures of *App3* and *App7*. Modifications (white boxes) of the linear capsule polymer backbones are introduced by separate and as-yet-unidentified enzymes. (b) Reactions catalyzed by the gene products Cps3B/Cps7B and Cps3D/Cps7D. (c) Schematic representation of region 2 of the capsule gene clusters of *App3* and *App7*.

GCTs have never been used to supply CDP-Gro for preparative-scale syntheses of polymers. For this study, we designed a novel enzymatic cascade using GCTs and TagF-like polymerases and hypothesize that it can provide enantiopure poly(glycosylglycerol-phosphate) at a preparative-scale for vaccine development.

## RESULTS

**Identification of GCTs in *App3* and *App7*.** Centerpiece of the envisioned synthesis cascade is a suitable GCT for the supply of enantiopure CDP-Gro. A number of bacterial GCTs were previously characterized and showed activity *in vitro*, e.g., the GCTs from *Bacillus subtilis* (16), *Staphylococcus aureus* (17, 18), *Enterococcus faecalis*, and *Listeria monocytogenes* (19). Apart from two exceptions (20), all GCTs belong to a larger family of cytidyltransferases comprising GCT, CTP:phosphoethanolamine cytidyltransferase

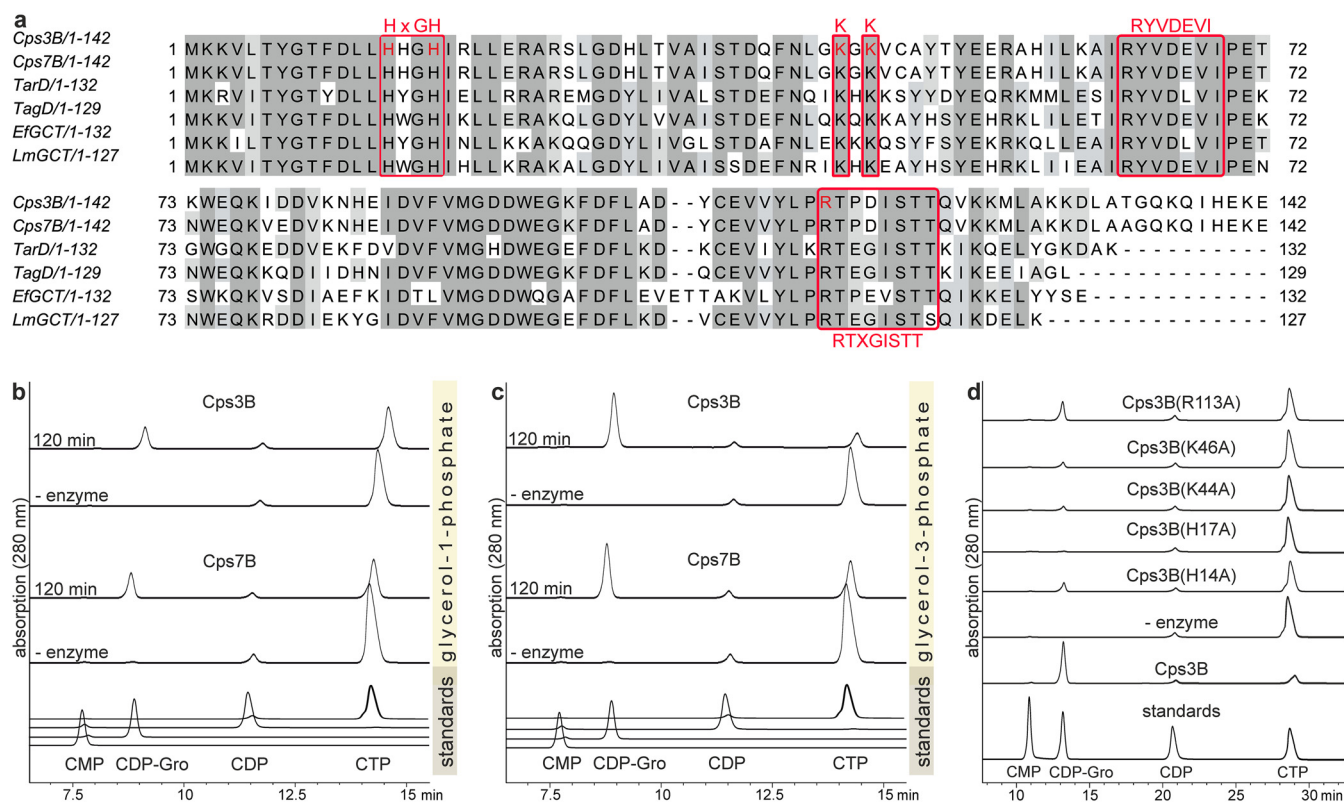


**FIG 2** Alignment of different GCT amino acid sequences and activity of Cps3B and Cps7B. (a) Amino acid sequence alignment of Cps3B (*App3*, GenBank ABY70165.1), Cps7B (*App7*, GenBank ACE62293.1), TarD (*S. aureus*, GenBank CAA60586.1), TagD (*B. subtilis*, GenBank AAA22843.1), GCT (*E. faecalis*, GenBank AA080975.1), and GCT (*L. monocytogenes*, GenBank AE016830). Identical amino acids are highlighted in gray, and conserved motifs and residues are boxed (in red). Residues mutated in Cps3B in this study are indicated by red text. (b and c) Substrate consumption in Cps3B and Cps7B reactions in the presence of Gro1P (b) or Gro3P (c) analyzed via HPLC-AEC coupled to UV detection. (d) Activity of Cps3B mutants analyzed by HPLC-AEC.

(ECT), CTP:2-C-methyl-D-erythritol-4-phosphate cytidyltransferase (CMS), and CTP: phosphocholine cytidyltransferase (CCT) (21). Members of this family contain two highly conserved sequences (Fig. 2a) involved in the binding of CTP: the HxGH motif, also identified in class I aminoacyl-tRNA synthetases, and the RTXGISTT motif, which is unique to the cytidyltransferase family (22). A third conserved motif, RYVDEVI, is part of the dimer interface (14). In TagD from *Bacillus subtilis*, several residues, such as His14 and His17 of the HxGH motif and Arg113 of the RTEGISTT motif, were shown to be essential for catalytic function (22). Two lysine residues, Lys44 and Lys46, were shown to interact with the negatively charged phosphates of CDP-Gro (23). The genes *cps3B* and *cps7B* from *App3* and *App7*, respectively, were predicted to encode glycerol-3-phosphate cytidyltransferases (15). They share 97% amino acid sequence identity with each other, ~70% sequence identity with TagD from *Bacillus subtilis*, ~61% identity with TarD from *Staphylococcus aureus*, ~60% identity with GCT from *Enterococcus faecalis*, and ~67% identity with GCT from *Listeria monocytogenes*. An alignment demonstrates that Cps3B and Cps7B indeed harbor all characteristic motives of the cytidyltransferase family (Fig. 2a).

To corroborate the putative GCT activity of Cps3B and Cps7B, we cloned, expressed, and purified both proteins. Activity was assessed by incubating recombinant Cps3B and Cps7B with their putative donor substrates CTP and GroP (both Gro1P and Gro3P were tested as potential substrates). We used high-performance liquid chromatography–anion-exchange chromatography (HPLC-AEC) coupled to UV detection (280 nm) to monitor the consumption and production of nucleotide substrates and products, respectively. Interestingly, CTP was consumed and CDP-Gro was produced in the presence of either GroP enantiomer (Fig. 2b and c). A precise quantitative assessment of GCT activity was beyond the scope of this study. Nevertheless, HPLC-AEC data indicate

(Fig. 2b and c) that CTP consumption and CDP-Gro production were higher in reaction mixtures containing Gro3P, suggesting a preference for this substrate. To corroborate that the enzymes belong to the cytidyltransferase family, residues presumably critical for activity of Cps3B were mutated to alanine. All mutants displayed reduced activity, indicated by low or absent CDP-Gro production and low CTP consumption (Fig. 2d).

**Production of enantiopure *App3* and *App7* capsule backbones in one-pot reactions.** Enzymatic one-pot reactions are powerful tools for the generation of complex biomolecules (24). Here, we investigated one-pot reactions of Cps3B+Cps3D and Cps7B+Cps7D. Reactions were performed in the presence of either GroP enantiomer, and UDP-Gal was added as second donor substrate for the polymerases (see reaction in Fig. 1b). Nucleotide substrate and product composition was analyzed prior to the addition of enzymes and after 120 min of incubation. The chromatograms demonstrate the consumption of CTP and the production of CDP-Gro (Fig. 3a and b). As expected, the nucleotide products CMP and UDP were detected, resulting from CDP-Gro and UDP-Gal consumption during polymer assembly. Again, the enzymes appear to prefer Gro3P over Gro1P, as indicated by higher levels of CMP and higher consumption of CTP. In agreement with this, Alcian blue/silver-stained PAGE gels corroborated that both polymerases were able to utilize Gro3P, while only Cps7D was able to assemble polymer from Gro1P (Fig. 3c). UDP, present in reaction mixtures containing Cps3D and Gro1P, results from enzyme-facilitated hydrolysis of UDP-Gal, which has been previously reported for TagF-like polymerases lacking appropriate donor and acceptor substrates (11, 25).

Despite the above demonstrated inability of Cps3D to utilize CDP-1-Gro, we previously showed that both Cps3D and Cps7D incorporated both enantiomers from a racemic mixture of CDP-Gro (11), creating an artificial polymer containing both GroP enantiomers. The nuclear magnetic resonance (NMR) chemical shifts of the resulting polymers (Fig. 3e, g, and h, blue correlations) diverge from the chemical shifts reported for the native polymers, especially for the atoms contributing to the glycosidic linkages (11). In the native *App7* polymer backbone, the glycosidic linkage is established between C1 of Gal and C1 of Gro3P (Fig. 3d, left) (12). In contrast, in the artificial repeating unit containing Gro1P, the glycosidic linkage connects C1 of Gal to C3 of Gro1P (Fig. 3d, right). As a result, the C1/H1 cross-peak observed for Gal in the artificial repeating unit is shifted downfield in the two-dimensional (2D)  $^1\text{H}$ - $^{13}\text{C}$  heteronuclear single quantum coherence (HSQC) spectrum (Fig. 3e, zoomed-in section) and cross-peaks for C3'/H3a' and C3'/H3b' of Gro appear in addition to the cross-peaks observed for C1'/H1a' and C1'/H1b' (Fig. 3e, blue spectrum). To investigate whether this heterogeneity disappears in polymers assembled from CDP-3-Gro using Cps7B and Cps7D, the one-pot reaction was upscaled to yield 5 mg of polymer, and 2D NMR analysis of the product was performed after purification via preparative AEC. Importantly, the  $^1\text{H}$  and  $^{13}\text{C}$  chemical shifts deduced from the 2D  $^1\text{H}$ - $^{13}\text{C}$  HSQC spectrum (Fig. 3e, red spectrum, and Table 1) and confirmed by 2D  $^1\text{H}$ - $^1\text{H}$  COSY (correlation spectroscopy),  $^1\text{H}$ - $^1\text{H}$  TOCSY (total correlation spectroscopy), and  $^1\text{H}$ - $^{31}\text{P}$  HMBC (heteronuclear multiple bond correlation) spectra (data not shown) are in perfect agreement with the chemical shifts reported for the natural polymer (12) and lack any heterogeneity.

The incorporation of both GroP enantiomers by Cps3D leads to the formation of three different repeating units appearing as distinct spin systems with well-isolated anomeric signals best visualized by  $^1\text{H}$ - $^1\text{H}$  NOESY (nuclear Overhauser enhancement spectroscopy) and  $^1\text{H}$ - $^{13}\text{C}$  HSQC (Fig. 3g and h) (11). The most intense and most downfield signal (5.23 ppm) results from the repeating unit in which the glycosidic linkage is formed with O2' of Gro3P (Fig. 3f, bottom, g, and h, and see Fig. S1 in the supplemental material). When Gro1P is incorporated, the glycosidic linkage is either correctly formed at O2' (Fig. 3f, top left) or misplaced at O3' (Fig. 3f, top right). The spin systems resulting from these repeating units are less abundant with well-isolated anomeric signals at 5.19 and 5.02 ppm, respectively. In contrast to the artificial polymer produced from racemic CDP-Gro, the polymer isolated from an upscaled one-pot reaction mixture containing Cps3B and Cps3D, together with enantiopure Gro3P, lacked any



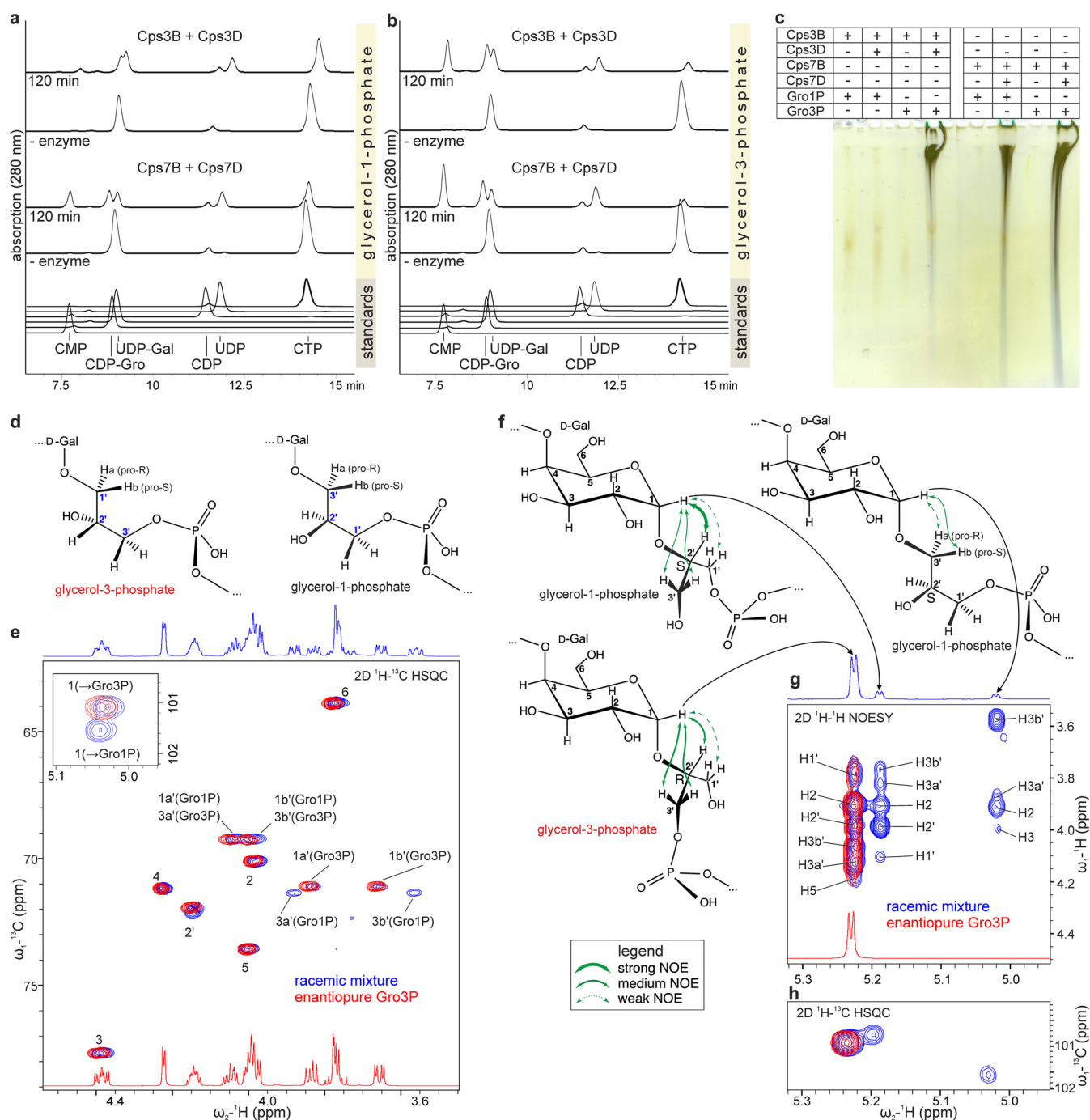


**FIG 3** Synthesis of enantiopure *App3* and *App7* polymers. (a and b) HPLC-AEC analysis of one-pot reaction mixtures containing GCTs, polymerases, and Gro1P or Gro3P, as indicated. Slight differences in retention time can result from different sample compositions (e.g., with or without enzyme). (c) Corresponding Alcian blue/silver-stained PAGE samples for visualization of synthesized polymer. (d) Chemical structures of Gro1P- and Gro3P-containing repeating units synthesized by Cps7D. (e) 2D  $^1\text{H}$ - $^{13}\text{C}$  HSQC spectra of polymer synthesized by Cps7D from racemic CDP-Gro (blue correlations) and enantiopure CDP-3-Gro (red correlations). (f) Chemical structures of Gro1P- and Gro3P-containing repeating units synthesized by Cps3D. Green arrows indicate NOEs (nuclear Overhauser effects, see legend). (g) 2D  $^1\text{H}$ - $^1\text{H}$  NOESY spectra of polymer synthesized by Cps3D from racemic CDP-Gro (blue correlations) and enantiopure (red correlations) CDP-3-Gro. (h) Corresponding 2D  $^1\text{H}$ - $^{13}\text{C}$  HSQC showing anomeric correlations. Reference spectra of racemic polymers were obtained from an earlier study (11).

heterogeneity and was in perfect agreement with the native *App3* polymer (13) (Fig. 3g and h, red spectrum, and Table 1). This finding suggests that also the native *App3* polymer is generated from CDP-3-Gro.

**GCTs can be combined with polymerases of other serotypes and genera.** TagF-like capsule polymerases can generate a large variety of structures, which are the basis

**TABLE 1**  $^1\text{H}$  and  $^{13}\text{C}$  chemical shifts of the Gro3P-containing polymers referenced to DSS (2,2-dimethyl-2-silapentanesulfonic acid)

Type	Chemical shifts (ppm)								
	Gal						Gro		
	C1/H1	C2/H2	C3/H3	C4/H4	C5/H5	C6/H6(+H6')	C1/H1(+H1')	C2/H2	C3/H3(+H3')
Cps3D	100.9/5.24	71.2/3.92	71.6/4.01	77.4/4.56	73.5/4.20	63.6/3.77	64.0/3.81	79.9/3.99	67.2/4.14+4.08
Cps7D	101.1/5.04	70.1/3.99	77.7/4.39	71.2/4.23	73.6/4.01	63.9/3.78	71.1/3.84+3.67	71.9/4.15	69.2/4.05+4.01
Cps11D	100.9/5.23	71.1/3.91	71.5/4.01	77.4/4.56	73.5/4.20	63.6/3.78	64.0/3.81	79.9/3.99	67.2/4.14+4.08
Bt188	101.2/5.00	71.2/3.91	71.7/3.99	77.5/4.55	73.5/4.04	63.7/3.78+3.75	71.1/3.82+3.64	72.0/4.12	69.4/4.06+3.98

for the serotyping of encapsulated pathogens (11). To investigate whether GCTs from one serotype can be combined with polymerases from other serotypes or other genera, a one-pot reaction mixture containing Cps7B and the TagF-like capsule polymerase Cps11D (*App11*) was set up. In addition, the TagF-like polymerase Bt188 (11), encoded by the as-yet-nonserotyped *Bibersteinia trehalosi* isolate USDA-ARS-USMARC-188 (26) was investigated. Being a major agent of pneumonia and septicemia in big horn and commercial sheep, *B. trehalosi* is becoming increasingly important for cattle farming as well (27, 28). Three of the four *B. trehalosi* serotypes described so far express glycosylglycerol-phosphate polymers assembled by TagF-like polymerases, making *B. trehalosi* an ideal target for extending the technology described here.

Both polymerases were analyzed by homology modeling in previous studies (11), but enzymatic activity had so far only been confirmed for Cps11D (29). Cps11D was cloned, expressed, and purified as previously described for Cps3D, which generates the same capsule polymer backbone (11). A coding sequence for Bt188 was reverse translated, synthesized, and purified from *E. coli* expression cultures via its C-terminal His<sub>6</sub> tag. One-pot reactions combining Cps7B with either Cps11D or Bt188 were incubated overnight, and substrate turnover was analyzed by HPLC-based AEC and via high-percentage PAGE. The combinations Cps3B/Cps7D and Cps7B/Cps3D were tested as well. In all reactions, donor substrates (CTP, CDP-Gro, and UDP-Gal) were completely converted to nucleotide products (CMP and UDP) (Fig. 4a), and polymer could be detected (Fig. 4b). To confirm the identity of the polymers, reactions were scaled up and analyzed by NMR. A  $^1\text{H}$  NMR spectrum was sufficient to demonstrate the identity between the polymers produced by Cps3D and Cps11D (Fig. 4d), corroborating the predicted activity of Cps11D. Importantly, the  $^1\text{H}$  and  $^{13}\text{C}$  chemical shifts deduced from a  $^1\text{H}$ - $^{13}\text{C}$  HSQC experiment of the polymer produced by Bt188 were in perfect agreement with published data of the native, de-O-acetylated polymer of *B. trehalosi* serotype T3 (30), indicating that this as-yet-nonserotyped isolate expresses a T3 polymer backbone (Fig. 4e and Table 1). In summary, the above presented experiments demonstrate that Cps3B and Cps7B can be successfully combined with various capsule polymerases in one-pot reactions to yield the desired polymer products.

**Exploiting the modular architecture of TagF-like polymerases.** The modular architecture of TagF-like capsule polymerases is one of the major advantages for exploiting these enzymes as biosynthesis tools. We previously showed that inactivation of one of the two catalytic domains of Cps7D leads to single-action transferases having either Gal-transferase or GroP-transferase activity (11). Combining the respective mutants restores polymerase activity to wild-type levels, corroborating that each domain is independent from the other with regard to activity and folding. To broaden the structural variety of polymers producible by TagF-like capsule polymerases, we investigated whether single-action transferases from different serotypes, e.g., the GroP-transferase activity of Cps3D and the Gal-transferase activity of Cps7D, could be combined to generate new, non-*App3/7* structures like the polymer backbone of *B. trehalosi* serotype T3 (*BtT3*) (Fig. 5a). A one-pot reaction mixture containing both single-action transferases was set up and analyzed by HPLC-AEC and PAGE. Indeed, substrate consumption was complete and polymer identical to that synthesized by Bt188 was produced (Fig. 5b and c) as shown by  $^1\text{H}$  NMR (Fig. 5d).

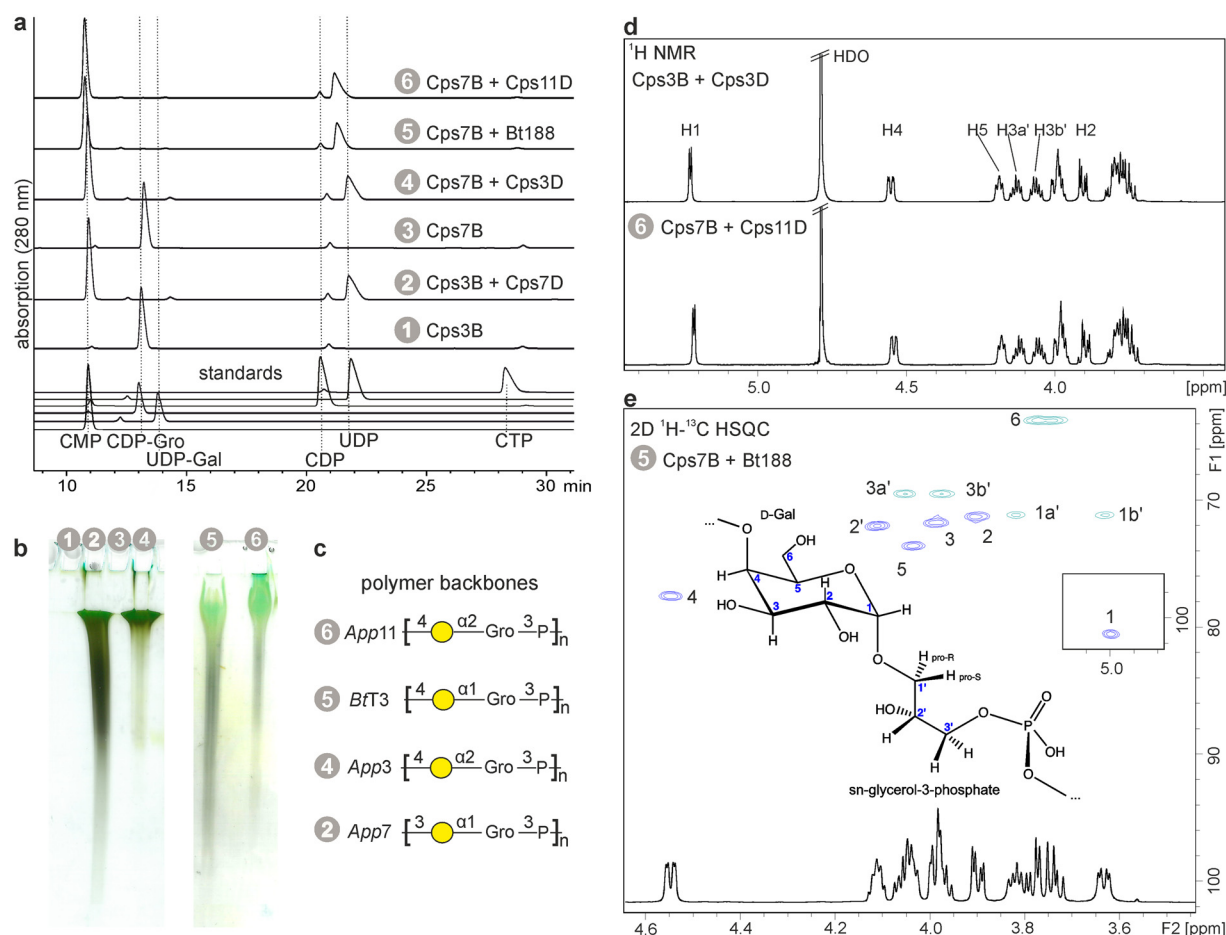


**FIG 4** Combining the GCTs Cps3B and Cps7B with polymerases of different serotypes and genera in one-pot reactions. (a) HPLC-AEC of one-pot reaction mixtures containing GCTs and polymerases, as indicated. Reactions 1 and 3 were used as positive controls for CDP-Gro production. (b and c) Corresponding polyacrylamide (PA) gel stained with Alcian blue/silver (b) and polymer structures (c). (d) <sup>1</sup>H NMR spectra of polymers synthesized in one-pot reaction mixtures containing GCTs and polymerases, as indicated. (e) 2D <sup>1</sup>H-<sup>13</sup>C HSQC spectrum of the polymer synthesized in a one-pot reaction mixture containing Cps7B and Bt188.

**Solid-phase synthesis.** Recently, our group established protocols for the tailored, enzymatic solid-phase synthesis of capsule polymers from *Neisseria meningitidis* serogroups A and X (31) and *A. pleuropneumoniae* serotype 1 (32). Here, we apply this approach to Cps7B and Cps7D (Fig. 6a). The proteins Cps7B-His<sub>6</sub> and MBP-Cps7D-His<sub>6</sub> (MBP [maltose-binding protein]) were expressed in *E. coli* and separately immobilized on Ni-NTA columns via their C-terminal His<sub>6</sub> tag. A reaction mixture containing CTP and Gro3P was circulated through the setup for several rounds (Fig. 6a, left), before the flowthrough was supplemented with UDP-Gal and transferred to the setup containing the Cps7D-loaded column (Fig. 6a, right). Samples were taken frequently to analyze reaction progress (Fig. 6b and c). As expected, immobilized Cps7B-His<sub>6</sub> and MBP-Cps7D-His<sub>6</sub> were active, as indicated by CDP-Gro (Fig. 6b), CMP/UDP (Fig. 6c), and polymer (Fig. 6d) production. Remaining UDP-Gal suggests a slight imbalance in the concentration ratio of both donor substrates (Fig. 6c). Small amounts of protein were detected in the collected fractions using Coomassie blue-stained SDS-PAGE (data not shown), and Western blot analyses demonstrate faint traces of free Cps7B-His<sub>6</sub> during CDP-Gro synthesis (Fig. 6e). However, these traces seem to be retained by the Cps7D-loaded Ni-NTA column, since they disappear in the fractions collected during polymer synthesis (Fig. 6f). Both constructs could be eluted with imidazole from their respective columns at the end of the experiment (see fraction E in Fig. 6e and f), emphasizing stable binding during the course of the experiment and



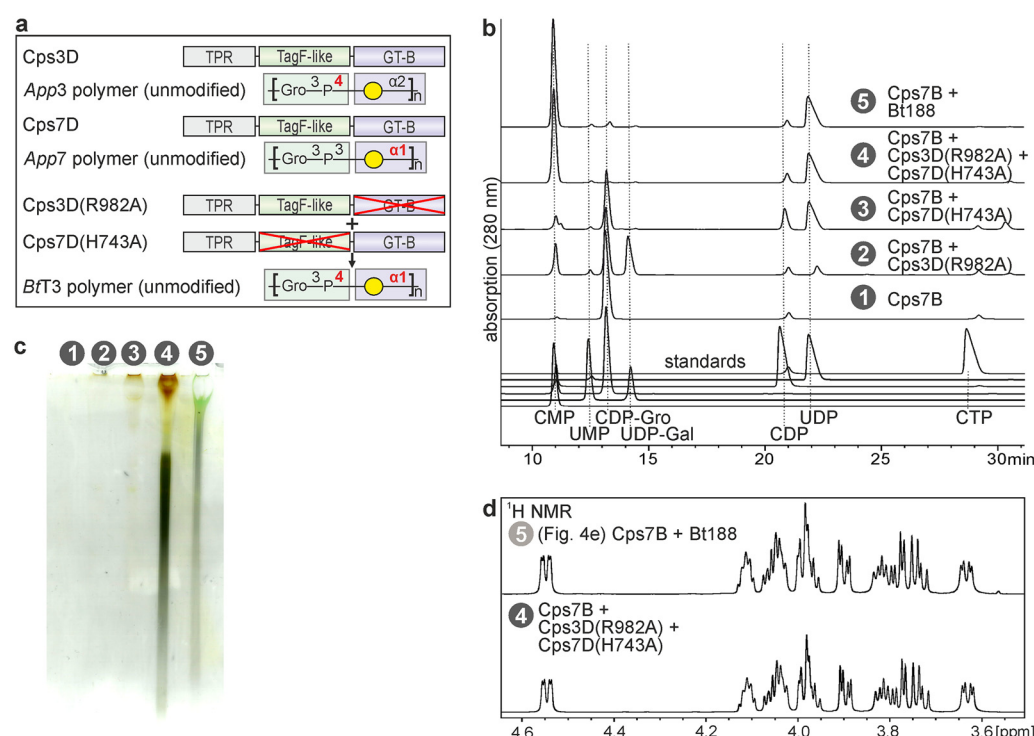


**FIG 5** Exploiting the modular architecture of TagF-like polymerases. (a) Domain organization of Cps3D and Cps7D, and the structural composition of their polymer products. Green and violet background colors indicate the domains that transfer the respective moiety. Combining the single-action Cps3D mutant Cps3D(R982A) that transfers Gro3P onto O4 of Gal and the single-action Cps7D mutant Cps7D(H743A) that generates a glycosidic linkage between Gal and O1 of Gro3P yields the polymer backbone of BtT3. (b) HPLC-AEC analysis of one-pot reaction mixtures containing Cps7B and single-action transferases, as indicated. Bt188 was used as a positive control. Single-action transferases alone were used as negative control. Elevated levels of CMP and UDP in samples 2 and 3, respectively, are due to enzyme facilitated hydrolysis catalyzed by the remaining active domain. (c) Corresponding PA gel stained with Alcian blue/silver. (d) <sup>1</sup>H NMR spectra of the polymer synthesized by Bt188 and the combination of Cps3D(R982A) and Cps7D(H743A).

indicating that solid-phase synthesis protocols are generally achievable using both catalysts.

**In situ CDP-Gro synthesis starting from UTP and glycerol.** The broad availability of vaccines is highly dependent on production costs (10). To evaluate whether the synthesis cascade could be started from the inexpensive, widely available substrates glycerol and nucleoside triphosphates (Fig. 7a), the putative glycerol kinase (Glpk; putative ATP:glycerol-3-phosphotransferase) (33) from App7 was cloned, expressed, purified, and tested in combination with the GCT Cps7B. We considered ATP, UTP, and CTP as putative donor substrates for App7-Glpk. Substrate uptake and CDP-Gro formation were analyzed by HPLC-AEC. Interestingly, most CDP-Gro was produced in the presence of UTP (Fig. 7b, reaction 2), even though the majority of characterized Glpks exhibit a preference for ATP (34). ATP and CTP were converted to ADP and CDP, respectively, but CDP-Gro levels were not detectable or low (Fig. 7b, reactions 1 and 3). This observation indicates that these nucleoside triphosphates were subject to enzyme facilitated hydrolysis but are not suitable substrates for *in situ* CDP-Gro production in the enzyme cascade. In a next step, we performed a one-pot reaction mixture containing Glpk, the GCT Cps7B and the polymerase Cps7D, together with their substrates glycerol, UTP, CTP, and UDP-Gal, to enable the production of polymer (see reaction scheme in Fig. 7a). As expected, the polymerase substrates UDP-Gal and CDP-Gro were converted into the products CMP, UDP (Fig. 7b, reaction 4) and polymer (Fig. 7c, reaction 4), demonstrating that the *in situ* synthesis of CDP-Gro is possible starting from glycerol and UTP.

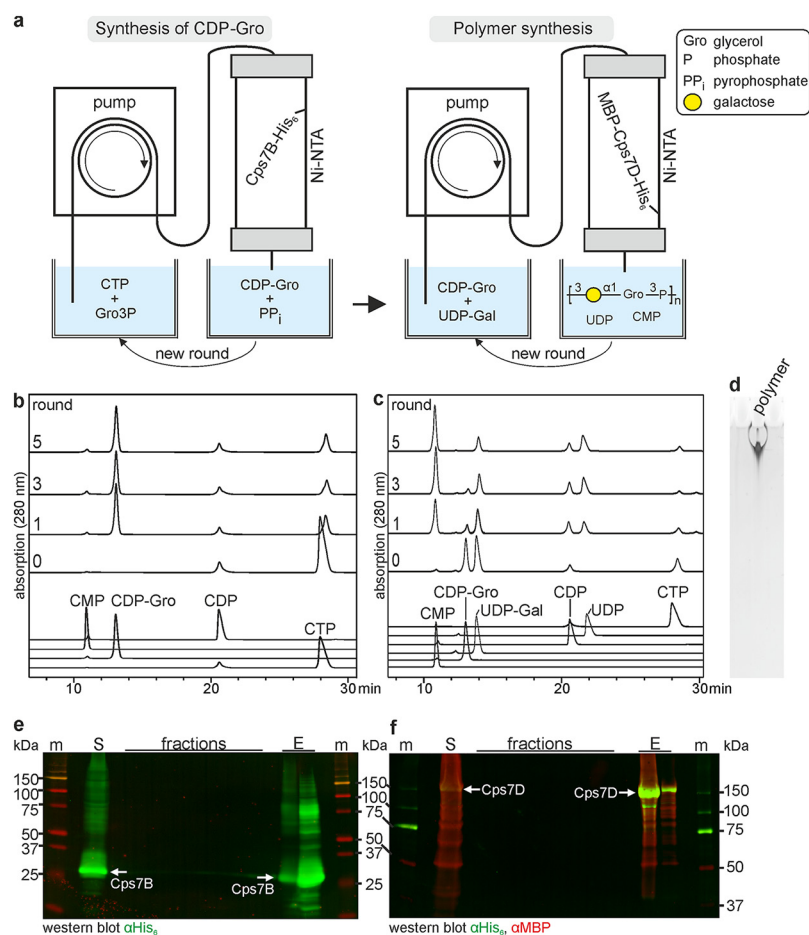


**FIG 6** Solid-phase synthesis of CDP-Gro and enantiopure *App7* polymer. (a) Schematic overview of the experimental setup. (b and c) HPLC-AEC analysis of the reaction mix before (0) and after the first (1), third (3) and fifth (5) round of circulation through Cps7B-loaded (b) and Cps7D-loaded (c) columns. (d) Alcian blue/silver-stained PA gel of polymer synthesized after round 5. (e and f) Western blot analysis of samples taken during CDP-Gro synthesis (e) and polymer synthesis (f). M, marker; S, supernatant; E, eluted protein; MBP, maltose-binding protein.

## DISCUSSION

This report presents the *in vitro* enzymatic production of complex glycerol-phosphate-containing group 2 capsule polymers from different Gram-negative bacteria. The initial focus was on the synthesis of nature-identical, enantiopure *App3* and *App7* capsule polymer backbones, which are assembled by the TagF-like polymerases Cps3D and Cps7D, respectively. To supply the commercially unavailable donor substrate CDP-Gro, the first aim was to establish an affordable and scalable CDP-Gro supply using the two putative GCTs Cps3B and Cps7B from *App3* and *App7*, respectively. Although Cps3B and Cps7B utilized both commercially available GroP enantiomers, it is unlikely that both precursors are present in *A. pleuropneumoniae*. *In vivo*, GroP is produced by the glycerol phosphate dehydrogenase (GPDH) from achiral dihydroxyacetone phosphate (DHAP), a central metabolite of glycolysis (35). In *Bacteria* (and *Eukarya*), this enzyme synthesizes Gro3P, whereas in *Archaea*, Gro1P is produced (35). As an exception from this rule, a GPDH (AraM) specific for Gro1P was recently identified in *B. subtilis* and shown to be involved in the generation of an archaea-type ether lipid (36, 37). However, the fact that the lipid synthetic pathway is restricted to the *Bacillales* suggests a single horizontal gene transfer event from an archaeal species rather than an ubiquitous occurrence of AraM in bacteria (37). A BLAST search against the *A. pleuropneumoniae* proteome using the AraM amino acid sequence as the query yielded a

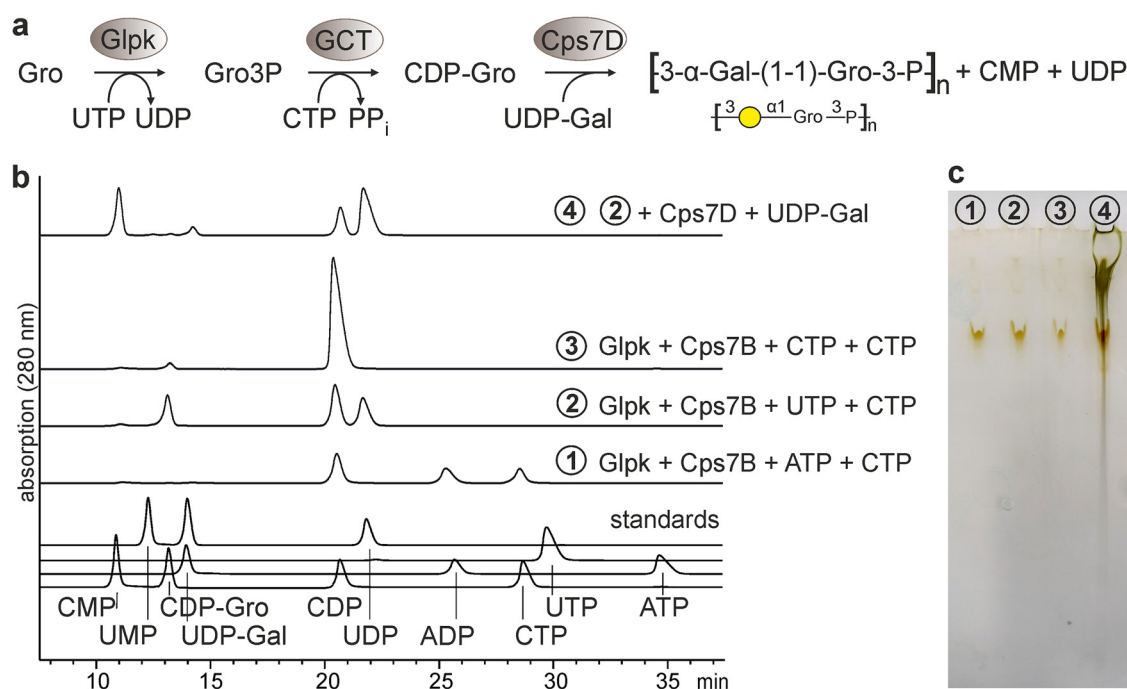


**FIG 7** One-pot polymer synthesis with *in situ* provision of CDP-Gro starting from UTP and glycerol. (a) Scheme of the enzymatic cascade showing all enzymes and substrates. (b) HPLC-AEC analysis of one-pot reaction mixtures containing enzymes and substrates, as indicated. (c) Corresponding Alcian blue/silver-stained PA gel. Bands visible in all reactions result from silver-stained enzymes.

single hit with 45% sequence identity. The identified enzyme, a putative 3-dehydroquinate synthase, is part of the shikimate pathway for the synthesis of aromatic amino acids, and is not known to harbor a GPDH activity (38).

Alternatively, GroP can be produced by glycerol kinase (Glpk), as presented here using Glpk from *App7*. Glpk is expressed in bacteria and heterotrophic archaea to allow the catabolic use of glycerol. To the best of our knowledge, it exclusively synthesizes Gro3P (39–41). Thus, it is reasonable to assume that free Gro1P is absent in the vast majority of bacteria. As a result, most studies assayed GCTs only in the presence of Gro3P. Only Rodrigues et al. (20) tested the GCTs AQ185 and AQ1368 from the Gram-negative bacterium *Aquifex aeolicus*, as well as one as-yet-unidentified GCT activity from lysates of the archaeon *Archaeoglobus fulgidus*, in the presence of both substrates. These researchers found AQ185 to be specific for Gro3P, whereas AQ1368 and the *A. fulgidus* enzymes utilized both substrates but showed a preference for Gro3P and Gro1P, respectively. Interestingly, the Gro3P-specific AQ185 belongs to the flavin adenine dinucleotide synthetase family. In contrast, the promiscuous AQ1368, like Cps3B and Cps7B, is part of the cytidyltransferase family. It is of note that the substrate ambiguity observed here makes Cps3B and Cps7B not only usable for the synthesis of Gro3P-containing bacterial structures but also for enzymatic reactions requiring CDP-1-Gro, e.g., during biosynthesis of archaean glycerophosphoinositol (20).

Despite the likely absence of CDP-1-Gro in bacteria, Gro1P has been found in surface structures such as lipoteichoic acid, phosphatidylglycerol, streptococcal rhamnose polysaccharides, and lipopolysaccharide (42–44). However, in all of these molecules the Gro1P moiety appears to originate from substrates other than CDP-1-Gro. For instance, during lipoteichoic acid synthesis, phosphatidylglycerol is formed after transfer of Gro3P and subsequent release of the sn-3-phosphoryl group from the resulting phosphatidylglycerol phosphate, retaining a Gro1P moiety that subsequently is transferred by the lipoteichoic acid synthase (45).

Similar to Cps3B and Cps7B, the polymerases Cps3D and Cps7D were able to utilize both GroP enantiomers from a racemic mixture of CDP-Gro, generating a mixed,

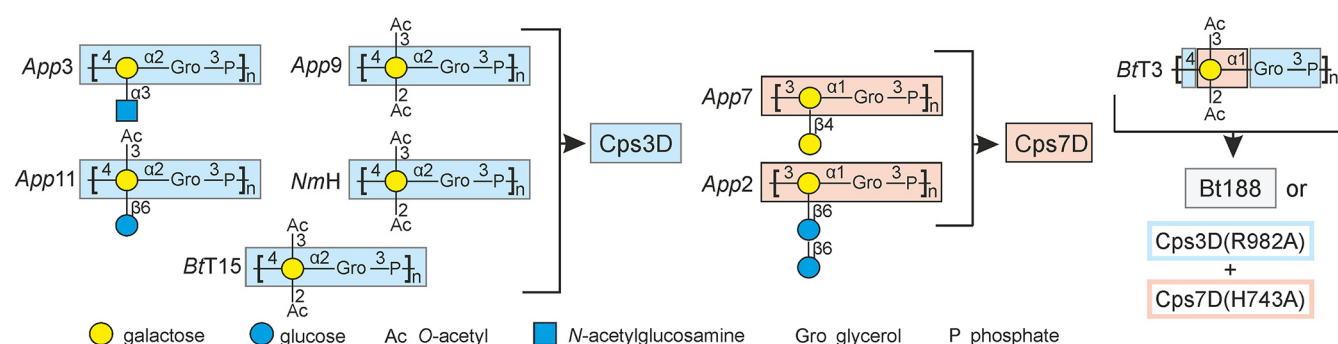


**FIG 8** Overview of capsule polymer backbones producible with enzyme-based protocols described in this study. The native polymer structures are described in the following references: *App3* (13), *App9* (70), *App11* (71), *NmH* (72), *BtT15* (73), *App7* (12), *App2* (74), and *BtT3* (30).

artificial polymer (11). However, in the present study it became clear that only Cps7D can build a polymer from enantiopure CDP-1-Gro, although the natural polymer exclusively contains Gro3P (12). We hypothesize that this promiscuity is possible because in the *App7* polymer the glycosidic linkage is formed via O1 of glycerol, which is two bonds away from the stereocenter at C2 (Fig. 1b). Interestingly, like Cps7D, the mammalian enzymes fukutin and fukutin-related protein that sequentially transfer two ribitol-phosphates during the synthesis of the laminin-binding epitope of *O*-mannosyl glycan, were also shown to accept CDP-1-Gro and CDP-3-Gro as the substrate (46). However, in this case, CDP-1-Gro was the better donor, presumably because the orientation of the hydroxyl group at the second carbon proximal to the phosphate group is the same in CDP-ribitol and CDP-1-Gro, but not in CDP-3-Gro (46). In contrast to Cps7D, Cps3D forms the glycosidic linkage directly with O2 at the stereocenter and was inactive in the presence of pure CDP-1-Gro. This finding clearly identifies CDP-3-Gro as the only possible substrate for Cps3D and additionally clarifies the stereochemistry of GroP in the *App3* capsular polysaccharide, which had not been elucidated so far (13).

The efficacy of *A. pleuropneumoniae* glycoconjugate vaccines could be shown in initial studies (47–49). However, these vaccines never came to market, presumably due to the high production costs associated with obtaining the polymer from pathogen cultures. To reduce production costs and improve the lot consistency and homogeneity of glycoconjugate vaccines in general, considerable effort has been made to develop alternative means for antigen provision, e.g., by chemical synthesis (50), *in vitro* (chemo)enzymatic synthesis (51), and *in vivo* enzymatic synthesis in engineered *E. coli* safety strains (52, 53). The construction of enzymatic synthesis routes and the detailed understanding of the biocatalysts involved is crucial for the latter two strategies. An advantage of enzymatic synthesis is that polymer assembly starts from highly pure substrates, which simplifies downstream processing. Importantly, TagF-like polymerases only require nucleotide-activated donor substrates to initiate polymerization, omitting the need to provide acceptor saccharides (11). Here, we developed two separate enzymatic approaches for *in vitro* polymer production: one-pot and solid-phase synthesis. Although both methods are scalable and attractive for biotechnological use, only solid-phase synthesis can allow the reuse of enzyme-loaded matrices and does not require separation of the biocatalysts from the final products (54, 55). To further reduce production costs and increase scalability, the enzymatic cascade was expanded to include Glpk and GCT (Fig. 7), allowing the synthesis of enantiopure CDP-3-Gro from inexpensive starting materials that are widely available in large quantities.

Due to the fact that several pathogens express identical poly(glycosylglycerol phosphate) capsule polymer backbones, Cps3D and Cps7D can be used to supply polymer antigens for *A. pleuropneumoniae* serotypes 2, 3, 7, 9, and 11; *B. trehalosi* serotype T15; and *Neisseria meningitidis* serogroup H (*NmH*) (Fig. 8). However, it is important to note that *in vivo*, these capsule polymer backbones are modified (12, 13). In group 2 capsule



biosynthesis systems, such modifications are usually introduced by separate enzymes after assembly and, depending on the pathogen, can be beneficial or detrimental for the immunological response induced by a glycoconjugate vaccine (56, 57). Although a few group 2 capsule-modifying *O*-acetyltransferases have been identified and characterized (58, 59), group 2 capsule-modifying glycosyltransferases are still unknown. Future studies will show if these enzymes can be integrated in the synthesis cascade and if the modifications are necessary for a functional *A. pleuropneumoniae* vaccine.

A recent publication (60) authored by vaccine manufacturers, regulatory authorities, research institutions, and independent researchers in the field of vaccine development defined the challenges for future glycoconjugate vaccine development and identified the inadequate understanding of the mechanisms by which the immune system interacts with these complex antigens as a major drawback for vaccine improvement. The authors emphasized the importance of developing economic production platforms and encouraged studies that assess how factors like oligosaccharide size and structure impact the induced immune response. The technology presented here can contribute to both points, since the avoidance of pathogen culture and less laborious polymer purification can reduce costs. Moreover, previous studies have shown that the two-domain architecture of TagF-like polymerases can be exploited for the sequential buildup of tailored oligosaccharides, if single-action transferases are immobilized on separate solid phases (32). The authors further discussed that the knowledge gained from studying glycoconjugate vaccines in surrogate animal models is limited and often not transferable to the immune response in humans, making it hard to deduce a mechanism of action for these vaccines in general (60). Glycoconjugate vaccines against, e.g., *A. pleuropneumoniae*, can be studied in pigs as their natural host organism, omitting the use of a surrogate animal model and allowing us to draw more accurate conclusions from studies analyzing how certain vaccine characteristics (e.g., carrier protein, chain length, and coupling chemistry) influence the induced immune response and how protection against the pathogen is achieved. Thus, the study of anti-*A. pleuropneumoniae* glycoconjugate vaccines made with the technology presented here might not only improve our knowledge of the still poorly understood cell-mediated immune responses against an *A. pleuropneumoniae* infection (4, 61) but can also contribute to a better understanding of the mechanism of action of glycoconjugate vaccines in general.

The value of easily adaptable vaccine production platforms that are pathogen-free and allow quick responses to novel diseases is impressively demonstrated by the current COVID-19 pandemic (62). We present here a highly versatile toolbox for antigen synthesis. This is ideal for vaccines against *A. pleuropneumoniae*, since the predominance of *A. pleuropneumoniae* serotypes can vary geographically and temporally (4), increasing the necessity for frequent adaptation of the vaccine antigen. The versatility of the presented platform can be even further increased by exploiting the modular architecture of TagF-like polymerases, which allows the creation of single-action transferases that in turn can be combined in *trans* with other single-action transferases to generate entirely new polymer structures. This tempts us to speculate that TagF-like polymerases might be exploitable for the (chemo)enzymatic synthesis of other phosphate-containing structures like Gram-positive wall teichoic acids or, due to the substrate promiscuity of Cps3B/7B and Cps7D, even for Gro1P-containing lipoteichoic acids and O antigens.

## MATERIALS AND METHODS

**Bioinformatics.** BLASTP (63) (protein-protein BLAST) searches were performed against the non-redundant protein sequence database. The sequence alignment was performed with Clustal Omega (64) using the UniProt website (<http://www.uniprot.org/align/>) (65) and annotated with Jalview (66). Bruker TopSpin version 4.0.7 was used to process NMR data. Sparky (T. D. Goddard and D. G. Kneller, SPARKY 3; University of California, San Francisco) was used to analyze and assign NMR data.

**General cloning.** All primers and restriction enzymes used in this study are listed in Tables S1 and S2 in the supplemental material. *cps3B/cps7B* and *cps11D* were amplified by PCR from heat-inactivated bacterial lysates (Table 2) and cloned into plasmids *p*ΔN37-csIB-His<sub>6</sub> (25) and *p*MBP-csxA-His<sub>6</sub> (67),

**TABLE 2** Strains and enzymes used in this study

Strain	Serotype	Protein	Accession no.
<i>Actinobacillus pleuropneumoniae</i> S1421	<i>App3</i>	Cps3B	GenBank, ABY70165.1
<i>Actinobacillus pleuropneumoniae</i> AP76	<i>App7</i>	Cps7B	GenBank, ACE62293.1
<i>Actinobacillus pleuropneumoniae</i> S1421	<i>App3</i>	Cps3D	GenBank, KY807157
<i>Actinobacillus pleuropneumoniae</i> AP76	<i>App7</i>	Cps7D	GenBank, ACE62291.1
<i>Actinobacillus pleuropneumoniae</i> 56153 <sup>a</sup>	<i>App11</i>	Cps11D	UniParc, UPI0001E49633
Nonserotyped <i>Bibersteinia trehalosi</i> strain USDA-ARS-USMARC-188 <sup>b</sup>		Bt188	GenBank, AHG82487.1
<i>Actinobacillus pleuropneumoniae</i> AP76	<i>App7</i>	Glpk	GenBank, ACE61051

<sup>a</sup>Frey and Nicolet (75), Xu et al. (15).<sup>b</sup>Harhay et al. (26).

respectively, replacing *cslB* and *csxA*, resulting in the constructs *pcps3B-His<sub>6</sub>*/*pcps7B-His<sub>6</sub>* and *pMBP-cps11D-His<sub>6</sub>*. The construction of Cps3D, Cps7D, and Cps7D (H743A) was described previously (11). The Bt188 amino acid sequence (GenBank AHG82487.1) was reverse translated into DNA (see Text S1 in the supplemental material), codon optimized for expression in *E. coli*, synthesized by General Biosystems, and cloned via NdeI/XhoI into expression vector pET-22b(+), resulting in the plasmid *pBt188-His<sub>6</sub>*. Single-amino-acid mutations in Cps3B and Cps3D were introduced using the Q5 site-directed mutagenesis kit (New England Biolabs) according to the manufacturer's guideline, and plasmids *pcps3B-His<sub>6</sub>* and *pMBP-cps3D-His<sub>6</sub>* (11) were used as the template, respectively. *Glpk* was amplified via PCR from heat-inactivated bacterial lysate (Table 2) and cloned via restriction-free cloning (68) into plasmid *pcps7B-His<sub>6</sub>*, replacing *cps7B*.

**Expression and purification of recombinant proteins.** Expression and purification of Cps3D, Cps7D, Cps11D, Bt188, Cps3D(R982A), and Cps7D(H743A) were performed as described previously (11, 25). Cps3B, Cps7B, all Cps3B mutants, and Glpk were purified accordingly, with the adjustment that the buffer contained 10 mM Tris-HCl (pH 8.0), 300 mM NaCl, and 10% glycerol (+ 500 mM imidazole for elution). The protein yield was determined spectrophotometrically using the theoretical extinction coefficients predicted by ProtParam (69).

#### Enzymatic reactions, HPLC-AEC analysis, and high-percentage polyacrylamide gel electrophoresis.

All enzymatic reactions were carried out with 1 to 2  $\mu$ M enzyme at 37°C in a total volume of 25 to 50  $\mu$ l of assay buffer (20 mM Tris-HCl [pH 8.0], 1 mM DTT [dithiothreitol], 10 mM MgCl<sub>2</sub>). The substrate concentration of CTP (Sigma), Gro1P and Gro3P (both Sigma), and, if required, UDP-Gal (Carbosynth) was 5 mM. In reaction mixtures containing Glpk, 5 mM substrates (CTP and ATP [Roche] and UTP [Sigma]) were used, and pyrophosphatase (0.003 U/ $\mu$ l; Invitrogen) was added. Glycerol was supplied from the enzymes' storage buffer, yielding 0.7% glycerol in the final reaction mixture. Samples for the high-performance liquid chromatography (HPLC) and PAGE analyses were taken prior to the addition of enzymes and after 2 h of incubation or after an overnight reaction. High-performance liquid chromatography-anion-exchange chromatography (HPLC-AEC) and PAGE analyses were performed as described previously (11, 29) with minor adjustments: The chromatograms shown in Fig. 2 and 3 were recorded using a linear elution gradient from 0 to 25% of mobile phase 2 over 14 min. The chromatograms shown in Fig. 2d and Fig. 4 to 7 were recorded with a linear elution gradient from 0 to 25% of mobile phase 2 over 42 min and 5  $\mu$ l of sample.

**Upscaling of polymer synthesis and purification.** Polymer (5 mg) was synthesized in one-pot reactions by combining GCTs and polymerases in reaction buffer (20 mM Tris-HCl [pH 8.0], 10 mM MgCl<sub>2</sub>, 1 mM DTT) supplemented with 5 mM concentrations of each donor substrate in a total volume of 3.2 ml at 37°C overnight. The amount of GCT ranged from 7.5 to 28 nmol, and 7.5 to 9 nmol of polymerase was used. Polymer was purified by AEC as described previously (11).

**NMR analyses.** NMR data were recorded on a Bruker Avance III HD 600-MHz spectrometer with a QXI room-temperature probe for <sup>1</sup>H/<sup>13</sup>C/<sup>15</sup>N/<sup>31</sup>P (Bruker Biospin, Germany) at 298 K in D<sub>2</sub>O as described previously (11).

**Solid-phase synthesis.** Expression of Cps7B and Cps7D was performed as described previously (11), solid-phase synthesis was performed according to published protocols (31, 32) with minor adjustments: 250 ml of *E. coli* M15 (pRep4) expression culture was used for coupling of enzymes to 1 ml Ni-NTA columns (Cytiva). The Cps7B-loaded column was thoroughly washed with binding buffer A (10 mM Tris-HCl [pH 8.0], 300 mM NaCl, 10% glycerol, 1 mM DTT). The Cps7D-loaded column was thoroughly washed with binding buffer B (50 mM Tris-HCl [pH 8.0], 500 mM NaCl, 1 mM DTT). Both columns were equilibrated in 20 mM Tris-HCl (pH 8.0), 10 mM MgCl<sub>2</sub>, and 1 mM DTT. Portions (5 ml) of the reaction mixture (equilibration buffer containing 6 mM CTP and 6 mM Gro3P) were circulated at a flow rate of 0.4 ml/min through a Cps7B-loaded column. After several rounds of circulation, the flowthrough was supplemented with 5 mM UDP-Gal and circulated through the Cps7D-loaded column (0.4 ml/min). Fractions were collected as indicated (Fig. 6). Recovery of enzymes was achieved using elution buffer (binding buffer A supplemented with 500 mM imidazole for Cps7B and binding buffer B supplemented with 500 mM imidazole for Cps7D). Samples were analyzed by using HPLC-AEC and Alcian blue/silver-stained PAGE as described above. Samples from Cps7B- and Cps7D-loaded columns were separated by SDS-PAGE (16 and 10%, respectively) and analyzed by Western immunoblotting as described previously (67) using anti-penta-His (Qiagen) and anti-MBP (antibodies-online) as primary antibodies and goat anti-mouse IR800 (LI-COR) and goat anti-rabbit IR680 (LI-COR) as secondary antibodies. Western blot bands were detected with the Odyssey infrared imaging system (LI-COR).

**Data availability.** All data are presented in the manuscript or supplemental material, including NMR chemical shifts (Table 1). Raw NMR data are available from the corresponding author upon request.

## SUPPLEMENTAL MATERIAL

Supplemental material is available online only.

**TEXT S1**, PDF file, 0.2 MB.

**FIG S1**, PDF file, 0.3 MB.

**TABLE S1**, PDF file, 0.3 MB.

**TABLE S2**, PDF file, 0.2 MB.

## ACKNOWLEDGMENTS

This study was funded by Deutsche Forschungsgemeinschaft (DFG, German Research Foundation) - project number 412824531.

A.B., M.B., T.F., R.G.-S., and C.L. have submitted patent applications in the field of vaccine development.

Christa Litschko: conceptualization, formal analysis, investigation, methodology, supervision, visualization, writing—original draft, writing—review and editing. Insa Budde: formal analysis, investigation, writing—review and editing. Monika Berger: investigation, writing—review and editing. Andrea Bethe: investigation, writing—review and editing. Julia Schulze: investigation, writing—review and editing. E. Alberto Alcalá Orozco: investigation, writing—review and editing. Reza Mahour: investigation, writing—review and editing. Peter Goettig: investigation, visualization, writing—review and editing. Jana Indra Fühling: investigation, writing—review and editing. Thomas Rexer: investigation, writing—review and editing. Rita Gerardy-Schahn: funding acquisition, resources, writing—review and editing. Mario Schubert: formal analysis, investigation, methodology, validation, writing—review and editing. Timm Fiebig: conceptualization, formal analysis, funding acquisition, investigation, methodology, project administration, supervision, visualization, writing—original draft, writing—review and editing.

## REFERENCES

1. Roca I, Akova M, Baquero F, Carlet J, Cavaleri M, Coenen S, Cohen J, Findlay D, Gyssens I, Heur OE, Kahlmeter G, Kruse H, Laxminarayan R, Liébana E, López-Cerero L, MacGowan A, Martins M, Rodríguez-Baño J, Rolain J-M, Segovia C, Sigauque B, Tacconelli E, Wellington E, Vila J. 2015. The global threat of antimicrobial resistance: science for intervention. *New Microbes New Infect* 6:22–29. <https://doi.org/10.1016/j.nmni.2015.02.007>.
2. Van Boeckel TP, Brower C, Gilbert M, Grenfell BT, Levin SA, Robinson TP, Teillant A, Laxminarayan R. 2015. Global trends in antimicrobial use in food animals. *Proc Natl Acad Sci U S A* 112:5649–5654. <https://doi.org/10.1073/pnas.1503141112>.
3. Loera-Muro A, Angulo C. 2018. New trends in innovative vaccine development against *Actinobacillus pleuropneumoniae*. *Vet Microbiol* 217:66–75. <https://doi.org/10.1016/j.vetmic.2018.02.028>.
4. Sassu EL, Bossé JT, Tobias TJ, Gottschalk M, Langford PR, Hennig-Pauka I. 2018. Update on *Actinobacillus pleuropneumoniae*: knowledge, gaps, and challenges. *Transbound Emerg Dis* 65:72–90. <https://doi.org/10.1111/tbed.12739>.
5. Stygar AH, Niemi JK, Oliviero C, Laurila T, Heinonen M. 2016. Economic value of mitigating *Actinobacillus pleuropneumoniae* infections in pig fattening herds. *Agric Syst* 144:113–121. <https://doi.org/10.1016/j.agsy.2016.02.005>.
6. Rappuoli R. 2018. Glycoconjugate vaccines: principles and mechanisms. *Sci Transl Med* 10:1–7.
7. Costantino P, Rappuoli R, Berti F. 2011. The design of semi-synthetic and synthetic glycoconjugate vaccines. *Expert Opin Drug Discov* 6:1045–1066. <https://doi.org/10.1517/17460441.2011.609554>.
8. Whitfield C, Wear SS, Sande C. 2020. Assembly of bacterial capsular polysaccharides and exopolysaccharides. *Annu Rev Microbiol* 74:521–543. <https://doi.org/10.1146/annurev-micro-011420-075607>.
9. Oldrini D, Fiebig T, Romano MR, Proietti D, Berger M, Tontini M, De Ricco R, Santini L, Morelli L, Lay L, Gerardy-Schahn R, Berti F, Adamo R. 2018. Combined chemical synthesis and tailored enzymatic elongation provide fully synthetic and conjugation-ready *Neisseria meningitidis* serogroup X vaccine antigens. *ACS Chem Biol* 13:984–994. <https://doi.org/10.1021/acscmbio.7b01057>.
10. Micoli F, Del Bino L, Alfini R, Carboni F, Romano MR, Adamo R. 2019. Glycoconjugate vaccines: current approaches towards faster vaccine design. *Expert Rev Vaccines* 18:881–895. <https://doi.org/10.1080/14760584.2019.1657012>.
11. Litschko C, Oldrini D, Budde I, Berger M, Meens J, Gerardy-Schahn R, Berti F, Schubert M, Fiebig T. 2018. A new family of capsule polymerases generates teichoic acid-like capsule polymers in gram-negative pathogens. *mBio* 9:e00641-18. <https://doi.org/10.1128/mBio.00641-18>.
12. Beynon LM, Perry MB, Richards JC. 1991. Structure of the capsular polysaccharide from *Actinobacillus pleuropneumoniae* serotype 7. *Carbohydr Res* 209:211–223. [https://doi.org/10.1016/0008-6215\(91\)80158-J](https://doi.org/10.1016/0008-6215(91)80158-J).
13. Altman E, Brisson JR, Perry MB. 1987. Structure of the capsular polysaccharide of *Haemophilus pleuropneumoniae* serotype 3. *Biochem Cell Biol* 65:960–967. <https://doi.org/10.1139/o87-125>.
14. Weber CH, Park YS, Sanker S, Kent C, Ludwig ML. 1999. A prototypical cytidyltransferase: CTP:glycerol-3-phosphate cytidyltransferase from *Bacillus subtilis*. *Structure* 7:1113–1124. [https://doi.org/10.1016/S0969-2126\(99\)80178-6](https://doi.org/10.1016/S0969-2126(99)80178-6).
15. Xu Z, Chen X, Li L, Li T, Wang S, Chen H, Zhou R. 2010. Comparative genomic characterization of *Actinobacillus pleuropneumoniae*. *J Bacteriol* 192:5625–5636. <https://doi.org/10.1128/JB.00535-10>.
16. Park YS, Sweitzer TD, Dixon JE, Kent C. 1993. Expression, purification, and characterization of CTP:glycerol-3-phosphate cytidyltransferase from *Bacillus subtilis*. *J Biol Chem* 268:16648–16654. [https://doi.org/10.1016/S0021-9258\(19\)85467-4](https://doi.org/10.1016/S0021-9258(19)85467-4).
17. Badurina DS, Zolli-Juran M, Brown ED. 2003. CTP:glycerol 3-phosphate cytidyltransferase (TarD) from *Staphylococcus aureus* catalyzes the cytidyl transfer via an ordered Bi-Bi reaction mechanism with micromolar *K<sub>m</sub>* values. *Biochim Biophys Acta* 1646:196–206. [https://doi.org/10.1016/S1570-9639\(03\)00019-0](https://doi.org/10.1016/S1570-9639(03)00019-0).

18. Fong DH, Yim VC-N, D'Elia MA, Brown ED, Berghuis AM. 2006. Crystal structure of CTP:glycerol-3-phosphate cytidylyltransferase from *Staphylococcus aureus*: examination of structural basis for kinetic mechanism. *Biochim Biophys Acta* 1764:63–69. <https://doi.org/10.1016/j.bbapap.2005.10.015>.
19. Meril AN, Friesen JA. 2012. Comparative kinetic analysis of glycerol 3-phosphate cytidylyltransferase from *Enterococcus faecalis* and *Listeria monocytogenes*. *Med Sci Monit* 18:BR427–BR434. <https://doi.org/10.12659/MSM.883535>.
20. Rodrigues MV, Borges N, Santos H. 2017. Glycerol phosphate cytidylyltransferase stereospecificity is key to understanding the distinct stereochemical compositions of glycerophosphoinositol in *Bacteria* and *Archaea*. *Appl Environ Microbiol* 83:e02462-16. <https://doi.org/10.1128/AEM.02462-16>.
21. Brault JP, Friesen JA. 2016. Characterization of cytidylyltransferase enzyme activity through high-performance liquid chromatography. *Anal Biochem* 510:26–32. <https://doi.org/10.1016/j.ab.2016.07.018>.
22. Park YS, Gee P, Sanker S, Schurter EJ, Zuiderweg ER, Kent C. 1997. Identification of functional conserved residues of CTP:glycerol-3-phosphate cytidylyltransferase: role of histidines in the conserved HXGH in catalysis. *J Biol Chem* 272:15161–15166. <https://doi.org/10.1074/jbc.272.24.15161>.
23. Patridge KA, Weber CH, Friesen JA, Sanker S, Kent C, Ludwig ML. 2003. Glycerol-3-phosphate cytidylyltransferase: structural changes induced by binding of CDP-glycerol and the role of lysine residues in catalysis. *J Biol Chem* 278:51863–51871. <https://doi.org/10.1074/jbc.M306174200>.
24. Wang Y, Ren H, Zhao H. 2018. Expanding the boundary of biocatalysis: design and optimization of *in vitro* tandem catalytic reactions for biochemical production. *Crit Rev Biochem Mol Biol* 53:115–129. <https://doi.org/10.1080/10409238.2018.1431201>.
25. Litschko C, Romano MR, Pinto V, Claus H, Vogel U, Berti F, Gerardy-Schahn R, Fiebig T. 2015. The capsule polymerase CslB of *Neisseria meningitidis* serogroup L catalyzes the synthesis of a complex trimeric repeating unit comprising glycosidic and phosphodiester linkages. *J Biol Chem* 290:24355–24366. <https://doi.org/10.1074/jbc.M115.678094>.
26. Harhay GP, McVey DS, Koren S, Phillippy AM, Bono J, Harhay DM, Clawson ML, Heaton MP, Chitko-McKown CG, Korlach J, Smith TPL. 2014. Complete closed genome sequences of three *Bibersteinia trehalosi* nasopharyngeal isolates from cattle with shipping fever. *Genome Announc* 2:e00084-14.
27. Brown S, Bycroft K, Adam K, Collett M. 2021. Acute fibrinous pleuropneumonia and septicaemia caused by *Bibersteinia trehalosi* in neonatal calves in New Zealand. *N Z Vet J* 69:51–57. <https://doi.org/10.1080/00480169.2020.1792372>.
28. Dassanayake RP, Shanthalingam S, Subramaniam R, Herndon CN, Bavananthasivam J, Haldorson GJ, Foreyt WJ, Evermann JF, Herrmann-Hoesing LM, Knowles DP, Srikanthar S. 2013. Role of *Bibersteinia trehalosi*, respiratory syncytial virus, and parainfluenza-3 virus in bighorn sheep pneumonia. *Vet Microbiol* 162:166–172. <https://doi.org/10.1016/j.vetmic.2012.08.029>.
29. Litschko C, Budde I, Berger M, Fiebig T. 2021. Exploitation of capsule polymerases for enzymatic synthesis of polysaccharide antigens used in glycoconjugate vaccines. *Methods Mol Biol* 2183:313–330. [https://doi.org/10.1007/978-1-0716-0795-4\\_16](https://doi.org/10.1007/978-1-0716-0795-4_16).
30. Richards JC, Leitch RA. 1990. Determination of the structure and absolute configuration of the glycerolphosphate-containing capsular polysaccharide of *Pasteurella haemolytica* serotype T3 by high-resolution nuclear magnetic resonance spectroscopy. *Can J Chem* 68:1574–1584. <https://doi.org/10.1139/v90-243>.
31. Fiebig T, Litschko C, Freiburger F, Bethe A, Berger M, Gerardy-Schahn R. 2018. Efficient solid-phase synthesis of meningococcal capsular oligosaccharides enables simple and fast chemoenzymatic vaccine production. *J Biol Chem* 293:953–962. <https://doi.org/10.1074/jbc.RA117.000488>.
32. Budde I, Litschko C, Fühling JI, Gerardy-Schahn R, Schubert M, Fiebig T. 2020. An enzyme-based protocol for cell-free synthesis of nature-identical capsular oligosaccharides from *Actinobacillus pleuropneumoniae* serotype 1. *J Biol Chem* 295:5771–5784. <https://doi.org/10.1074/jbc.RA120.012961>.
33. Lin EC. 1976. Glycerol dissimilation and its regulation in bacteria. *Annu Rev Microbiol* 30:535–578. <https://doi.org/10.1146/annurev.mi.30.100176.002535>.
34. Koga Y, Morikawa M, Haruki M, Nakamura H, Imanaka T, Kanaya S. 1998. Thermostable glycerol kinase from a hyperthermophilic archaeon: gene cloning and characterization of the recombinant enzyme. *Protein Eng* 11:1219–1227. <https://doi.org/10.1093/protein/11.12.1219>.
35. Koga Y. 2014. From promiscuity to the lipid divide: on the evolution of distinct membranes in *Archaea* and *Bacteria*. *J Mol Evol* 78:234–242. <https://doi.org/10.1007/s00239-014-9613-4>.
36. Guldan H, Matysik F-M, Bocola M, Sterner R, Babinger P. 2011. Functional assignment of an enzyme that catalyzes the synthesis of an archaea-type ether lipid in bacteria. *Angew Chem Int Ed Engl* 50:8188–8191. <https://doi.org/10.1002/anie.201101832>.
37. Guldan H, Sterner R, Babinger P. 2008. Identification and characterization of a bacterial glycerol-1-phosphate dehydrogenase: Ni<sup>2+</sup>-dependent AraM from *Bacillus subtilis*. *Biochemistry* 47:7376–7384. <https://doi.org/10.1021/bi8005779>.
38. Nunes JES, Duque MA, de Freitas TF, Galina L, Timmers LFSM, Bizarro CV, Machado P, Basso LA, Ducati RG. 2020. *Mycobacterium tuberculosis* Shikimate pathway enzymes as targets for the rational design of anti-tuberculosis drugs. *Molecules* 25:1259. <https://doi.org/10.3390/molecules25061259>.
39. Nishihara M, Yamazaki T, Oshima T, Koga Y. 1999. *sn*-Glycerol-1-phosphate-forming activities in Archaea: separation of archaeal phospholipid biosynthesis and glycerol catabolism by glycerophosphate enantiomers. *J Bacteriol* 181:1330–1333. <https://doi.org/10.1128/JB.181.4.1330-1333.1999>.
40. Williams TJ, Allen M, Tschitschko B, Cavicchioli R. 2017. Glycerol metabolism of haloarchaea. *Environ Microbiol* 19:864–877. <https://doi.org/10.1111/1462-2920.13580>.
41. Villanueva L, Schouten S, Damsté JSS. 2017. Phylogenomic analysis of lipid biosynthetic genes of Archaea shed light on the “lipid divide.” *Environ Microbiol* 19:54–69. <https://doi.org/10.1111/1462-2920.13361>.
42. Gründling A, Schneewind O. 2007. Synthesis of glycerol phosphate lipoteichoic acid in *Staphylococcus aureus*. *Proc Natl Acad Sci U S A* 104:8478–8483. <https://doi.org/10.1073/pnas.0701821104>.
43. Shashkov AS, Yang B, Senchenkova SN, Perepelov AV, Liu B, Knirel YA. 2016. Structures and genetics of biosynthesis of glycerol 1-phosphate-containing O-polysaccharides of *Escherichia coli* O28ab, O37, and O100. *Carbohydr Res* 426:26–32. <https://doi.org/10.1016/j.carres.2016.03.011>.
44. Edgar RJ, van Hensbergen VP, Ruda A, Turner AG, Deng P, Le Breton Y, El-Sayed NM, Belew AT, McIver KS, McEwan AG, Morris AJ, Lambeau G, Walker MJ, Rush JS, Korotkov KV, Widmalm G, van Soerge NM, Korotkova N. 2019. Discovery of glycerol phosphate modification on streptococcal rhamnose polysaccharides. *Nat Chem Biol* 15:463–471. <https://doi.org/10.1038/s41589-019-0251-4>.
45. Walter A, Unsleber S, Rismondo J, Jorge AM, Peschel A, Gründling A, Mayer C. 2020. Phosphoglycerol-type wall and lipoteichoic acids are enantiomeric polymers differentiated by the stereospecific glycerophosphodiesterase GlpQ. *J Biol Chem* 295:4024–4034. <https://doi.org/10.1074/jbc.RA120.012566>.
46. Imae R, Many H, Tsumoto H, Osumi K, Tanaka T, Mizuno M, Kanagawa M, Kobayashi K, Toda T, Endo T. 2018. CDP-glycerol inhibits the synthesis of the functional O-mannosyl glycan of  $\alpha$ -dystroglycan. *J Biol Chem* 293:12186–12198. <https://doi.org/10.1074/jbc.RA118.003197>.
47. Byrd W, Harmon BG, Kadis S. 1992. Protective efficacy of conjugate vaccines against experimental challenge with porcine *Actinobacillus pleuropneumoniae*. *Vet Immunol Immunopathol* 34:307–324. [https://doi.org/10.1016/0165-2427\(92\)90172-M](https://doi.org/10.1016/0165-2427(92)90172-M).
48. Byrd W, Kadis S. 1992. Preparation, characterization, and immunogenicity of conjugate vaccines directed against *Actinobacillus pleuropneumoniae* virulence determinants. *Infect Immun* 60:3042–3051. <https://doi.org/10.1128/IAI.60.8.3042-3051.1992>.
49. Andresen LO, Jacobsen MJ, Nielsen JP. 1997. Experimental vaccination of pigs with an *Actinobacillus pleuropneumoniae* serotype 5b capsular polysaccharide-tetanus toxoid conjugate. *Acta Vet Scand* 38:283–293. <https://doi.org/10.1186/BF03548491>.
50. Schumann B, Bahr HS, Parameswarappa SG, Reppe K, Wahlbrink A, Govindan S, Kaplonek P, Pirofski L, Witzenthalm M, Anish C, Pereira CL, Seeberger PH. 2017. A semisynthetic *Streptococcus pneumoniae* serotype 8 glycoconjugate vaccine. *Sci Transl Med* 9:eaf5347. <https://doi.org/10.1126/scitranslmed.aaf5347>.
51. Fiebig T, Romano MR, Oldrini D, Adamo R, Tontini M, Brogioni B, Santini L, Berger M, Costantino P, Berti F, Gerardy-Schahn R. 2016. An efficient cell free enzyme-based total synthesis of a meningococcal vaccine candidate. *NPJ Vaccines* 1:16017. <https://doi.org/10.1038/npjvaccines.2016.17>.
52. Tytgat HLP, Lin C, Levasseur MD, Tomek MB, Rutschmann C, Mock J, Liebscher N, Terasaka N, Azuma Y, Wetter M, Bachmann MF, Hilvert D, Aebi M, Keys TG. 2019. Cytoplasmic glycoengineering enables biosynthesis of nanoscale glycoprotein assemblies. *Nat Commun* 10:5403. <https://doi.org/10.1038/s41467-019-13283-2>.
53. Harding CM, Nasr MA, Scott NE, Goyette-Desjardins G, Nothaft H, Mayer AE, Chavez SM, Huynh JP, Kinsella RL, Szymanski CM, Stallings CL, Segura M, Feldman MF. 2019. A platform for glycoengineering a polyvalent



- pneumococcal bioconjugate vaccine using *Escherichia coli* as a host. *Nat Commun* 10:891. <https://doi.org/10.1038/s41467-019-08869-9>.
54. Datta S, Christena LR, Rajaram YRS. 2013. Enzyme immobilization: an overview on techniques and support materials. *Biotech* 3:1–9. <https://doi.org/10.1007/s13205-012-0071-7>.
  55. Mohamad NR, Marzuki NHC, Buang NA, Huyop F, Wahab RA. 2015. An overview of technologies for immobilization of enzymes and surface analysis techniques for immobilized enzymes. *Biotechnol Biotechnol Equip* 29:205–220. <https://doi.org/10.1080/13102818.2015.1008192>.
  56. Fusco PC, Farley EK, Huang C-H, Moore S, Michon F. 2007. Protective meningococcal capsular polysaccharide epitopes and the role of O acetylation. *Clin Vaccine Immunol* 14:577–584. <https://doi.org/10.1128/CVI.00009-07>.
  57. Enotarpi J, Tontini M, Balocchi C, van der Es D, Auberger L, Balducci E, Carboni F, Proietti D, Casini D, Filippov DV, Overkleef HS, van der Marel GA, Colombo C, Romano MR, Berti F, Costantino P, Codeé JDC, Lay L, Adamo R. 2020. A stabilized glycomimetic conjugate vaccine inducing protective antibodies against *Neisseria meningitidis* serogroup A. *Nat Commun* 11:4434. <https://doi.org/10.1038/s41467-020-20120-4>.
  58. Fiebig T, Cramer JT, Bethe A, Baruch P, Curth U, Fühling JI, Buettner FFR, Vogel U, Schubert M, Fedorov R, Mühlenhoff M. 2020. Structural and mechanistic basis of capsule O-acetylation in *Neisseria meningitidis* serogroup A. *Nat Commun* 11:4723. <https://doi.org/10.1038/s41467-020-18464-y>.
  59. Berti F, De Ricco R, Rappuoli R. 2018. Role of O-acetylation in the immunogenicity of bacterial polysaccharide vaccines. *Molecules* 23:1340. <https://doi.org/10.3390/molecules23061340>.
  60. Avci F, Berti F, Dull P, Hennessey J, Pavliak V, Prasad AK, Vann W, Wacker M, Marcq O. 2019. Glycoconjugates: what it would take to master these well-known, yet little-understood immunogens for vaccine development. *mSphere* 4:e00520-19. <https://doi.org/10.1128/mSphere.00520-19>.
  61. Ramjeet M, Deslandes V, Gouré J, Jacques M. 2008. *Actinobacillus pleuropneumoniae* vaccines: from bacterins to new insights into vaccination strategies. *Anim Health Res Rev* 9:25–45. <https://doi.org/10.1017/S1466252307001338>.
  62. Krammer F. 2020. SARS-CoV-2 vaccines in development. *Nature* 586:516–527. <https://doi.org/10.1038/s41586-020-2798-3>.
  63. Boratyn GM, Camacho C, Cooper PS, Coulouris G, Fong A, Ma N, Madden TL, Matten WT, McGinnis SD, Merezuk Y, Raytselis Y, Sayers EW, Tao T, Ye J, Zaretskaya I. 2013. BLAST: a more efficient report with usability improvements. *Nucleic Acids Res* 41:W29–W33. <https://doi.org/10.1093/nar/gkt282>.
  64. Sievers F, Wilm A, Dineen D, Gibson TJ, Karplus K, Li W, Lopez R, McWilliam H, Remmert M, Söding J, Thompson JD, Higgins DG. 2011. Fast, scalable generation of high-quality protein multiple sequence alignments using Clustal Omega. *Mol Syst Biol* 7:539. <https://doi.org/10.1038/msb.2011.75>.
  65. Boutet E, Lieberherr D, Tognolli M, Schneider M, Bansal P, Bridge AJ, Poux S, Bougueleret L, Xenarios I. 2016. UniProtKB/Swiss-Prot, the manually annotated section of the UniProt KnowledgeBase: how to use the entry view. *Methods Mol Biol* 1374:23–54. [https://doi.org/10.1007/978-1-4939-3167-5\\_2](https://doi.org/10.1007/978-1-4939-3167-5_2).
  66. Waterhouse AM, Procter JB, Martin DMA, Clamp M, Barton GJ. 2009. Jalview Version 2: a multiple sequence alignment editor and analysis workbench. *Bioinformatics* 25:1189–1191. <https://doi.org/10.1093/bioinformatics/btp033>.
  67. Fiebig T, Berti F, Freiburger F, Pinto V, Claus H, Romano MR, Proietti D, Brogioni B, Stummeyer K, Berger M, Vogel U, Costantino P, Gerardy-Schahn R. 2014. Functional expression of the capsule polymerase of *Neisseria meningitidis* serogroup X: a new perspective for vaccine development. *Glycobiology* 24:150–158. <https://doi.org/10.1093/glycob/cwt102>.
  68. Bond SR, Naus CC. 2012. RF-Cloning.org: an online tool for the design of restriction-free cloning projects. *Nucleic Acids Res* 40:W209–W213. <https://doi.org/10.1093/nar/gks396>.
  69. Gasteiger E, Gattiker A, Hoogland C, Ivanyi I, Appel RD, Bairoch A. 2003. ExPASy: the proteomics server for in-depth protein knowledge and analysis. *Nucleic Acids Res* 31:3784–3788. <https://doi.org/10.1093/nar/gkg563>.
  70. Beynon LM, Richards JC, Perry MB. 1992. Nuclear-magnetic-resonance analysis of the capsular antigen of *Actinobacillus pleuropneumoniae* serotype 9. Its identity with the capsular antigen of *Escherichia coli* K62 (K2ab), *Neisseria meningitidis* serogroup H and *Pasteurella haemolytica* serotype T15. *Eur J Biochem* 210:119–124. <https://doi.org/10.1111/j.1432-1033.1992.tb17398.x>.
  71. Perry MB, Altman E, Brisson J-R, Beynon LM, Richards JC. 1990. Structural characteristics of the antigenic capsular polysaccharides and lipopolysaccharides involved in the serological classification of *Actinobacillus (Haemophilus) pleuropneumoniae* strains. *Serodiagn Immunother Infect Dis* 4:299–308. [https://doi.org/10.1016/0888-0786\(90\)90018-J](https://doi.org/10.1016/0888-0786(90)90018-J).
  72. Kaaden A, Doorn-van Wakeren JIM, Kamerling JP, Vliegenthart JFG, Tiesjema RH. 1984. Structure of the capsular antigen of *Neisseria meningitidis* serogroup H. *Eur J Biochem* 141:513–519. <https://doi.org/10.1111/j.1432-1033.1984.tb08222.x>.
  73. Adlam C, Knights JM, Mugridge A, Lindon JC, Williams JM, Beesley JE. 1985. Purification, characterization and immunological properties of the capsular polysaccharide of *Pasteurella haemolytica* serotype T15: its identity with the K62 (K2ab) capsular polysaccharide of *Escherichia coli* and the capsular polysaccharide of *Neisseria meningitidis*. *J Gen Microbiol* 131:1963–1972. <https://doi.org/10.1099/00221287-131-8-1963>.
  74. Altman E, Brisson JR, Perry MB. 1987. Structural studies of the capsular polysaccharide from *Haemophilus pleuropneumoniae* serotype 2. *Biochem Cell Biol* 65:414–422. <https://doi.org/10.1139/o87-053>.
  75. Frey J, Nicolet J. 1990. Hemolysin patterns of *Actinobacillus pleuropneumoniae*. *J Clin Microbiol* 28:232–236. <https://doi.org/10.1128/JCM.28.2.232-236.1990>.